



Hydroxyapatite based and anodic Titania nanotube biocomposite coatings: Fabrication, characterization and electrochemical behavior



Shahab Ahmadi, Iman Mohammadi, S.K. Sadrnezhaad *

Department of Materials Science and Engineering, Sharif University of Technology, P.O. Box 11155-9466, Tehran, Iran

ARTICLE INFO

Article history:

Received 17 July 2015

Revised 18 December 2015

Accepted in revised form 19 December 2015

Available online 21 December 2015

Keywords:

Titanium alloy

Anodizing

Hydroxyapatite

Electrochemical deposition

Nano-biocomposite

TiO₂ nanotubes

ABSTRACT

The main challenges of biological implants are suitable strength, adhesion, biocompatibility and corrosion resistance. This paper discusses fabrication, characterization and electrochemical investigation of anodized Ti6Al4V without and with a hydroxyapatite (HA) layer, HA/TiO₂ nanoparticles (NPs) and HA/TiO₂ nanotubes (HA/anodized). X-ray diffraction (XRD), field emission scanning electron microscopy (FE-SEM) and energy dispersive spectroscopy (EDS) were used to characterize and compare properties of different samples. Dense HA with uniform distribution and 12.8 ± 2 MPa adhesive strength enhanced to 19.2 ± 4 MPa by the addition of TiO₂ nanoparticles and enhanced to 23.1 ± 4 MPa by the deposition of a TNT interlayer was fabricated by an anodic oxidation process. EIS analysis divulged the polarization behavior of various layers formed on a Ti6Al4V substrate. Electrochemical measurements indicated polarization passivation due to incorporation of TiO₂ nanoparticles to HA. Hydroxyapatite on a TNT layer revealed lower corrosion resistance than a HA/TiO₂ nanoparticle sample due to the vacuolar nature of TNT conformation. The passivation current density of the Ti6Al4V alloy coated with a HA/TiO₂ nanocomposite (0.125 μA/cm²) was less than 1% of the bare substrate.

© 2015 Elsevier B.V. All rights reserved.

1. Introduction

Titanium and its alloys have attractive properties like strength, lightness, passivation and biocompatibility [1–5] which introduce them as appropriate materials for biomedical applications. Localized corrosion and ion release, however, are due to their detracting behaviors [6–9]. Because of inadequate bioactivity, most metallic implants need surface modification for the enhancement of bioactivity and hard-tissue osseointegration [10–14].

Hydroxyapatite (Ca₁₀(PO₄)₆(OH)₂) is the major inorganic component of natural bone and its presence in biomedical coatings can support hard-tissue ingrowth [15–17]. Hydroxyapatite (HA) is widely used as a coating biomaterial of dental and orthopedic implants [18–22]. Nevertheless, its interfacial adhesion to its substrate is relatively weak [23,24]. Recent studies have indicated that the use of titanium oxide (TiO₂) in the coating structure can improve the adhesion and corrosion behavior of the contacting layer [14,23,25–28]. In some cases, this oxide can stand as an intermediate layer between the hydroxyapatite deposit and the substrate. A TiO₂ layer can form by anodization. Porosity presence in a TiO₂ layer can enhance HA adhesion and produce suitable cell anchorage circumstances [29–31].

Previous researchers have shown substantial improvement by direct addition of TiO₂ nanoparticles into the HA layer [25,28–30]. This has

attracted much attention due to its bonding strength, good adhesion and corrosion resistance [14,23,25,28–30]. Expectation of drastic improvements in multilayer limb behavior by TiO₂ nanoparticle addition to the HA layer has motivated us to run further in-depth research on the subject. Titanium based anodized alloys coated with HA seem beneficial for biomedical applications plus nanoparticle extra returns. In spite of all promising gains, to the best of the authors' knowledge, no comparative study has previously been made available on different HA/TiO₂ configurations deposited on a Ti6Al4V substrate. The purpose of this study is to construct, characterize and compare bioengineering properties of Ti6Al4V alloy with and without various anodization, HA deposition and HA/TiO₂ nanocomposite formation processes. In order to study the electrochemical behavior and adhesion strength, the anodized, HA deposited and HA/TiO₂ nanoparticle combined samples were compared with the untreated samples.

2. Experimental procedure

Prior to electrochemical treatments, the specimens were polished by mechanical grinding from P600 to P2000 by SiC emery paper, 0.3 and 0.05% Al₂O₃ (~200 nm size) suspensions and then diamond paste. Fig. 1 illustrates a scanning electron microscopy image of the polished Ti6Al4V alloy surface. The shiny samples were cleaned by sonication in acetone for 10 min at 60 °C, then cleaned with ethanol in an ultrasonic bath for 5 min and rinsed with deionized water. They finally were dried with a stream of flowing air.

* Corresponding author.

E-mail address: sadrnezhaad@sharif.edu (S.K. Sadrnezhaad).

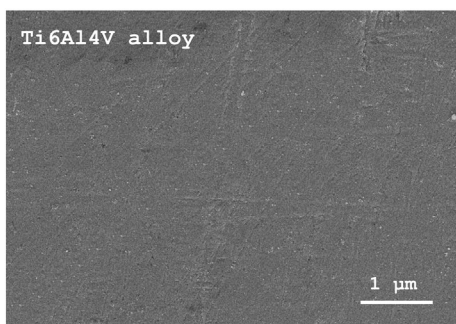


Fig. 1. Scanning electron microscopy images of the polished Ti6Al4V alloy surface.

2.1. TiO₂ nanotube production during electrochemical anodization process

Anodic oxidation was accomplished by using 1 M (NH₄)₂SO₄ electrolyte solution containing 0.5 wt.% NH₄F at the room temperature. The electrochemical setup consisted of a conventional two-electrode configuration with a SS 316L plate with a size of 6 × 2.5 cm and a thickness of 1 mm working as a cathode and a Ti6Al4V strip as anode. The electrochemical process involved a potential ramp from an open circuit potential (OCP) to 25 V with a sweeping rate of 25 mV/s followed by holding at the final potential for 2700 s. The samples were rinsed with deionized water and finally dried in flowing air.

2.2. Pulse electrodeposition of calcium phosphate

For electrochemical coating, both anodized and bare Ti6Al4V plates were placed in the cathode position (as substrate of HA/anodized Ti6Al4V and HA coatings, respectively) with a SS 316L plate functioning as the counter electrode. The electrolyte contained 0.042 M Ca(NO₃)₂, 0.025 M (NH₄)₂HPO₄, 0.1 M NaNO₃ and 2000 ppm H₂O₂. NaNO₃ was added to the electrolyte for the improvement of the ionic strength and H₂O₂ was added to suppress the H₂ evolution for dense deposit formation. The electrolyte pH was adjusted in the range of 5.5 to 6.5 by the addition of sodium hydroxide (NaOH) and nitric acid (HNO₃) at 60 °C.

To fabricate a HA/TiO₂ nanocomposite, 10 g/L TiO₂ powder with an irregular shape in the range of 80–120 nm (Merck Co. Ltd.) was also added to the electrolyte solution. In order to achieve a uniform and adherent deposition, a current density of $J_{\text{on}} = 1 \text{ mA/cm}^2$ was applied for 2 s (t_{on}), a resting time of $t_{\text{off}} = 5 \text{ s}$ ($J_{\text{off}} = 0 \text{ mA/cm}^2$) was implemented and the procedure was periodically repeated. The electrolyte temperature was adjusted at 60 °C, total procedure time was 60 min, and deposition process was done using a potentiostat/galvanostat pulsing current produced by a pulse rectifier (SL 2/25 PCS, I.R. Iran) as illustrated

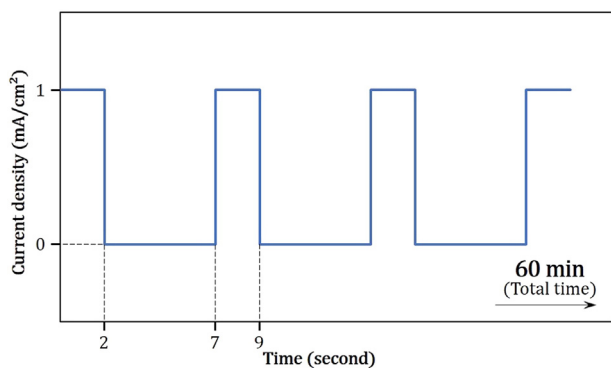


Fig. 2. Pulsating regime for electrodeposition of hydroxyapatite. Deposition at current density of $J_{\text{on}} = 1 \text{ mA/cm}^2$ for $t_{\text{on}} = 2 \text{ s}$ followed by breaking time of $t_{\text{off}} = 5 \text{ s}$ at $J_{\text{off}} = 0 \text{ mA/cm}^2$ for a total period of 60 min.

in Fig. 2. It should be noted that the prepared solution was dispersed by ultrasonic microwaves for 2 h in order to achieve a homogeneous suspension and stirred during the electrodeposition process in order to fabricate uniform layers and homogeneous deposition of TiO₂ nanoparticles into the hydroxyapatite matrix.

At the end of deposition, the sample was dried and then heated up to 120 °C by a 3 °C/min temperature rate. It was held at 120 °C for 2 h and then at 480 °C for 2 h, again. The purpose of heat treatment was the enhancement of calcium phosphate crystallinity and phase transformation of TiO₂ from amorphous to anatase configuration [32–35].

2.3. Bonding strength

The bonding strength of a deposit with substrate was measured according to ASTM F1044-05 standard. The uniaxial tensile load was applied to the deposit which was bonded to the substrate surface with the epoxy resin using an electromechanical testing system (Model 5565, Instron Co.) at a crosshead speed of 10 mm/min. The size of the samples used for the bonding strength tests was 30 × 30 × 1 mm. Five measurements were done for each deposit and the mean value was reported to determine the bonding strength.

2.4. Electrochemical behavior in body-simulated fluid (SBF) solution

Potentiodynamic polarization and electrochemical impedance spectroscopic (EIS) tests were carried out by a potentiostat apparatus (Autolab, PGSTAT302N) and EG&G (model 273A) respectively having a conventional three-electrode cell (saturated calomel electrode as reference, graphite plate (30 × 20 × 2 mm in size) as counter electrode and test specimen as the working electrode) for determination of the electrochemical behavior of the samples with and without surface modification. The working electrode consisted of a disk having an active surface area of 1 cm² and all other areas being isolated by an electrolyte-proof ring.

Potentiodynamic polarization tests were performed in the potential range of −0.8 to 1.2 V (vs. Ag/AgCl) at a scan rate of 1 mV/s. EIS studies were carried out in the frequency range of 10^{−2}–10⁵ Hz by using a 10 mV peak-to-peak sinusoidal potential amplitude. For acquiring spectra at the OCP, seven points per frequency decade was recorded. The data was analyzed by CorrView and ZSimpWin V3.40 software. Reproducibility check was done by three times repetition of the experiments. The test electrolyte was simulated body fluid (SBF) having pH = 7.4 and chemical composition indicated in Table 1. Prior to the electrochemical measurement, each sample was immersed into SBF for 30 min in order for OCP establishment.

2.5. Morphology and phase structure characterizations

Morphologies of the surface coatings were inspected by high vacuum FE-SEM model SIGMA/VP ZEISS. Before FE-SEM observation, Au was sputtered on the surface of the specimens. For each coating, three FE-SEM images were taken. Thickness measurements were done at four

Table 1

Chemical composition of the simulated body fluid (SBF) used in the electrochemical tests.

Component	Concentration (g/L)
NaCl	8.035
(CH ₂ OH) ₃ CNH ₂ (Tris)	6.118
NaHCO ₃	0.355
MgCl ₂ ·2H ₂ O	0.311
CaCl ₂	0.292
K ₂ HPO ₄ ·3H ₂ O	0.231
KCl	0.225
Na ₂ SO ₄	0.072
HCl (1 M)	39 mL/L

different regions per image. Average figure was reported. Crystal structures of the samples were analyzed by X-ray diffraction (XRD) (X'Pert Pro MPD, PANalytical) using Cu K α radiation of $\lambda = 1.5418 \text{ \AA}$, 2θ angle of $20\text{--}90^\circ$, scanning rate of 0.02°s^{-1} , time steps of 20 s and an X'Pert Highscore plus software data analysis system.

3. Results and discussion

3.1. FE-SEM micrographs

The top and cross-sectional FE-SEM micrographs of the anodized surface of Ti6Al4V alloy are shown in Fig. 3. Growth of the TiO₂ nanotubes perpendicular to the surface of the anodized sample is clearly observable in the figure. The layer has an average total thickness of $\sim 760 \text{ nm}$, nanotube mean wall-thickness of 23.7 nm , nanotube mean inner diameter of 95 nm and nanotube mean outer diameter of 170 nm .

The morphology of different HA-based layers coated on Ti6Al4V alloy is shown in Fig. 4 ((a, b) pure hydroxyapatite, (c, d) HA/anodized and (e, f) HA/TiO₂ nanocomposite).

Fig. 4a and b show that the nanostructured HA consists of both planar and rod-like microstructures. According to Fig. 4c and d, the HA deposit on an anodized sample consists of thin planes that stood on each other. Fig. 4e and f show a HA deposit with titanium oxide nanoparticles having an 80 to 120 nm diameter. It is interesting to point out that hydroxyapatite layers in nanotubes of titanium dioxide (Fig. 4c and d) are dense and uniform. In order to evaluate distribution of TiO₂ nanoparticles into the deposited layer, mapping of the elements was carried out by EDS. Fig. 5 indicates the FE-SEM image and the EDS dot map of different elements in the HA/TiO₂ nanocomposite deposition.

From the EDS mapping, it is understood that the TiO₂ nanoparticles are distributed uniformly throughout the surface layer. This can increase adhesion strength and integrity of the layer.

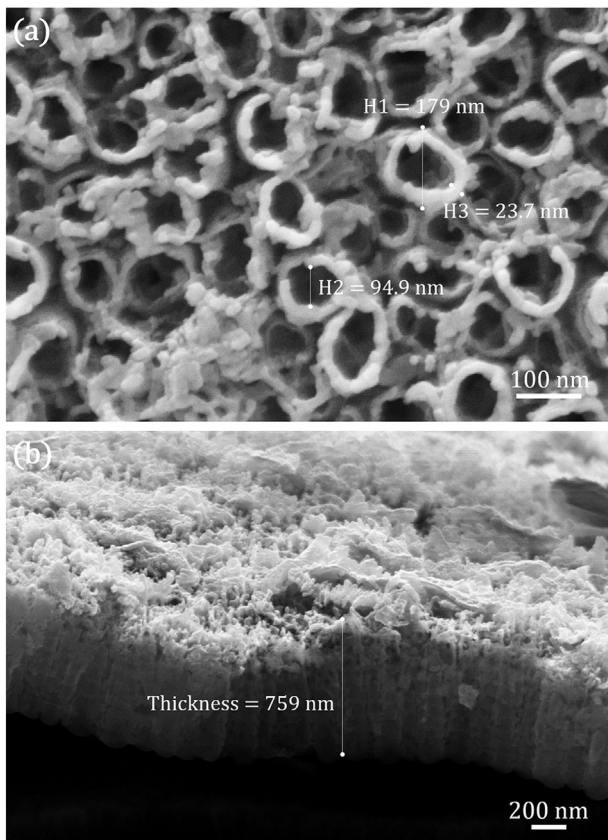


Fig. 3. The FE-SEM images of titanium oxide nanotubes formed by anodic oxidation of Ti6Al4V alloy viewed from: (a) top and (b) side of the sample.

3.2. Bonding strength

The bonding strength of the deposited hydroxyapatite with the Ti6Al4V substrate was $12.8 \pm 2 \text{ MPa}$. The corresponding value for a HA/TiO₂ nanocomposite was $19.2 \pm 4 \text{ MPa}$ and for HA/anodized the value measured $23.1 \pm 4 \text{ MPa}$. The results of bonding strength tests are indicated as a bar graph image with the corresponding standard deviations in Fig. 6. This shows that the presence of TiO₂ nanoparticles in the HA-based coating can drastically enhance the adhesion strength of the hydroxyapatite to the substrate. Possible reasons are:

- Reinforcement of the cohesive strength of HA with titanium oxide particles due to rough surface topography at the HA/TiO₂ nanoparticle interface.
- Formation of a HA/TiO₂ compact layer due to void filling.
- The presence of TiO₂ nanoparticles into the hydroxyapatite layer could relax residual stresses. In HA deposition, these stresses generally cause microcrack formation which degrades coating strength.

The highest bonding strength of $23.1 \pm 4 \text{ MPa}$ of a HA/anodized Ti6Al4V sample can thus be attributed to (a) HA/nanotube anchoring [36], (b) strengthening adhesion at the HA/anodized alloy interface [11–14] and (c) mechanical interlocking which provides compatible scaffolding [36]. Existence of TNTs as a middle oxide layer in the HA/anodized double layer improves the interfacial cohesion by superior chemical bonding of Titania with the substrate.

3.3. Corrosion behavior

Potentiodynamic polarization curves of different specimens are compared in Fig. 7. Two significant factors concerning corrosion potential (E_{corr}) and passivation current density (i_{pass}) are calculated from these curves. E_{corr} is a thermodynamic parameter that shows the chemical potential of the substance [37,38]. Moreover, according to the passivation behavior of coatings, corrosion susceptibility at the potential range of 200 to 600 mV (vs. SCE) was measured from passivation current density (i_{pass}). E_{corr} and i_{pass} values describing the corrosion behavior of the samples in SBF solution are summarized in Table 2. It would be mentioned that a more positive corrosion potential together with the smaller passivation current density result in higher corrosion resistance of the coating.

The data given in Table 2 depicts that the passivation current density of the Ti6Al4V substrate increases by anodizing ($18.96 \mu\text{A}/\text{cm}^2$ vs $32.28 \mu\text{A}/\text{cm}^2$) and corrosion potential decreases to -651 mV (vs. SCE). Improper corrosion behavior of the anodized sample is correlated to a permeable structure of the oxide layer formed on the Ti6Al4V substrate. However, the HA/TiO₂ nanocomposite-coated sample benefits from the lowest passivation current density as compared to the other specimens.

As is seen in Table 2, the passivation current density of the Ti6Al4V alloy with a HA/TiO₂ nanocomposite coating is $0.125 \mu\text{A}/\text{cm}^2$ (less than 1% of the bare substrate). Corrosion potential of the HA/TiO₂ nanocomposite coated sample is -264 mV (vs. SCE) which means that HA/TiO₂ nanocomposite deposition has noble potential.

According to Table 2, the presence of a hydroxyapatite deposit in the middle TNT layer of the HA/anodized sample improves the corrosion behavior of the sample but not as much as the sample containing only a HA coating. It is due to the fact that the hydroxyapatite layer in the TNTs prevents transport of ions and electrons to the deposit/electrolyte interface and retards self-regeneration of a protective TiO₂ layer. Oxygen passage through open pores results in less corrosion protection of the substrate.

Fig. 7 illustrates the corrosion behavior of different samples at 200 to 600 mV (vs. SCE). The body potential range defined by Velten et al. [40] (400 to 500 mV) is highlighted in the figure. In accordance with the

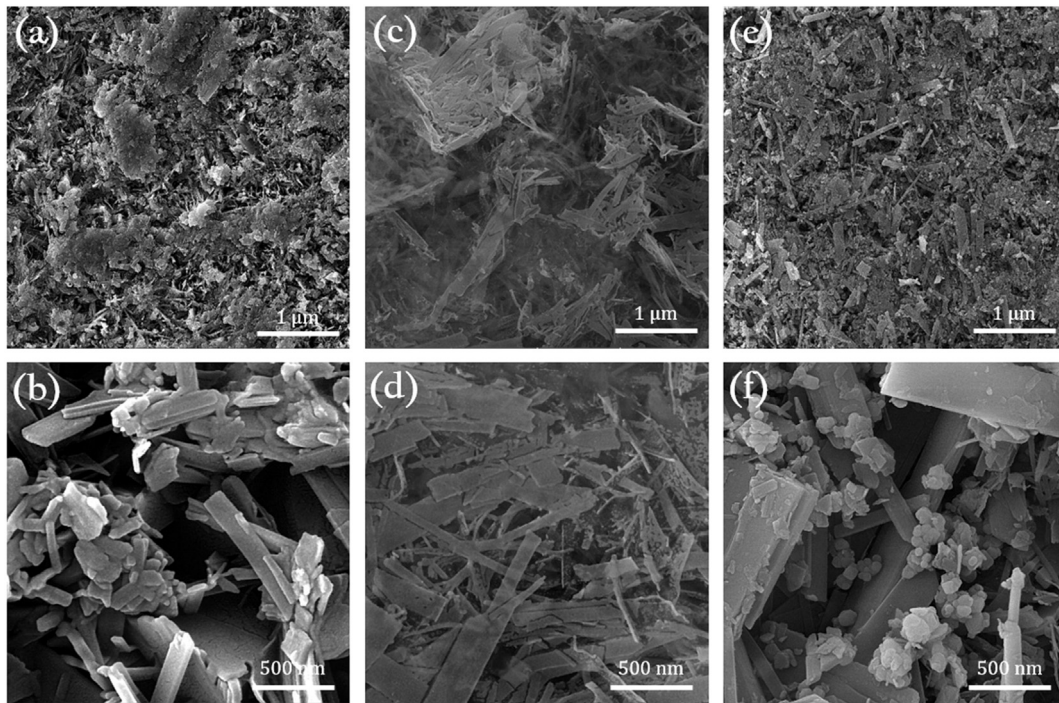


Fig. 4. FE-SEM micrographs of (a, b) deposited hydroxyapatite, (c, d) HA/anodized Ti6Al4V and (e, f) HA/TiO₂ nanocomposite all on Ti6Al4V alloy.

information given in Fig. 7 and Table 2, HA/TiO₂ nanocomposite coating demonstrates the lowest passivation current density at the acceptable corrosion potential and is thus introduced as an appropriate protective coating. Deposits having a hydroxyapatite coating generally have a smaller corrosion current density and nobler shift in the potential than the samples without HA. This is associated with the fact that calcium phosphates are inherently less soluble and have higher chemical stability. This effect can also be described by the “open-defects mechanism”, first suggested by Anawati et al. [39]. Deposition of uncompressed HA on a substrate results in the allowance of open-defects for the free flow of species that results in easy access of oxygen to the substrate surface and self-regeneration of a protective oxide layer which protects the sample from corrosion [39]. This assertion is not true for a

bare substrate which has a larger corrosion current. The anodized Ti6Al4V sample shows the worst corrosion behavior. This can be attributed to its highly porous structure.

3.4. Electrochemical impedance spectroscopy (EIS)

In order to study the electrochemical behavior of the deposits in more details and confirm the results obtained from the polarization tests, electrochemical impedance spectroscopy was performed on the samples (Figs. 8 and 9). Nyquist representation of the impedance diagram obtained for the untreated Ti6Al4V alloy, anodized, hydroxyapatite deposited, HA/anodized and HA/TiO₂ nanocomposite samples are presented in Fig. 8. A quantitative comparison between polarization

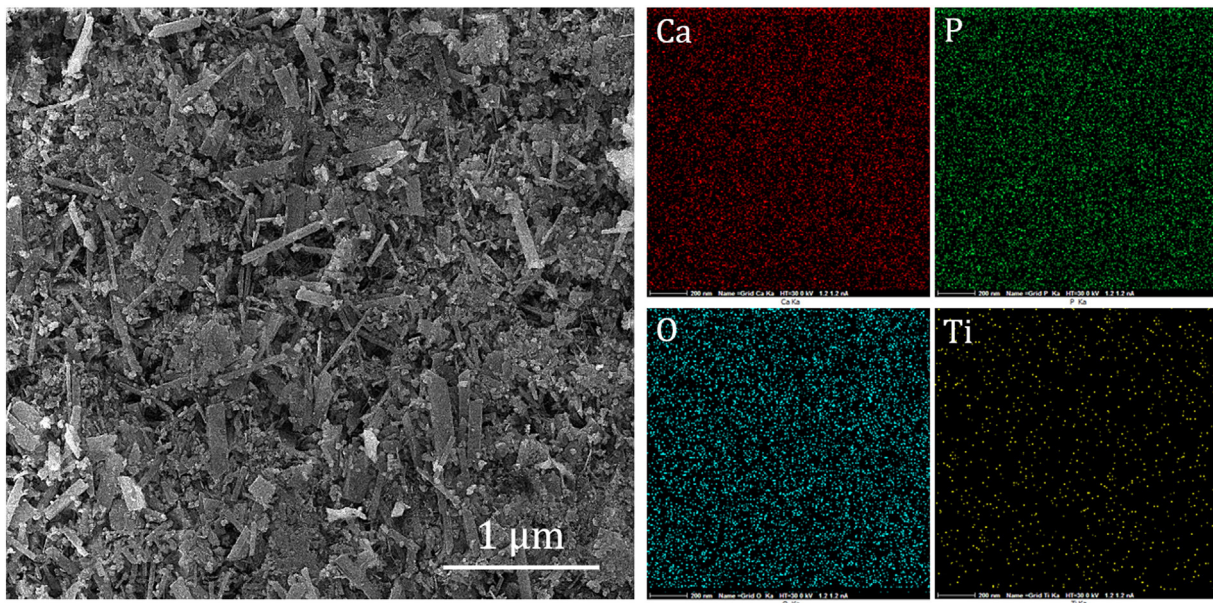


Fig. 5. Field emission scanning electron microscope image and EDS mapping of Ca, O, P and Ti in a HA/TiO₂ nanocomposite layer.

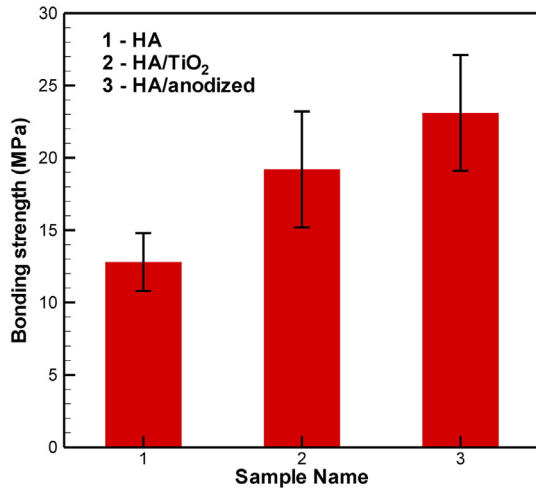


Fig. 6. Results of bonding strength tests for HA-based coatings deposited on Ti6Al4V alloy.

data and the results pertinent to the Nyquist plots ends up with similar conclusions. Capacitance loop diameter (Fig. 8) and Z modulus (Fig. 9a) of the HA/TiO₂ is substantially greater than that of other samples.

The specific polarization resistance was calculated following the fitting of the impedance experimental results by using the equivalent circuit displayed in Fig. 10a–e considering a solid electrode (untreated Ti6Al4V alloy, anodized, hydroxyapatite deposited, HA/anodized and HA/TiO₂ nanocomposite coatings) in contact with SBF electrolyte solution.

Due to the surface heterogeneities of the treated samples, as shown in Fig. 4a–f, a constant-phase element Q is used to fit the data instead of a pure capacitor C. These circuit elements obey the following equation [41]:

$$Q = C\omega^{\alpha-1} \tag{1}$$

where ω is the angular frequency and α is a number varying between 0 and 1 ($\alpha = 1$ for a pure-capacitor behavior) [41]. In Fig. 10a–e, R_s is the

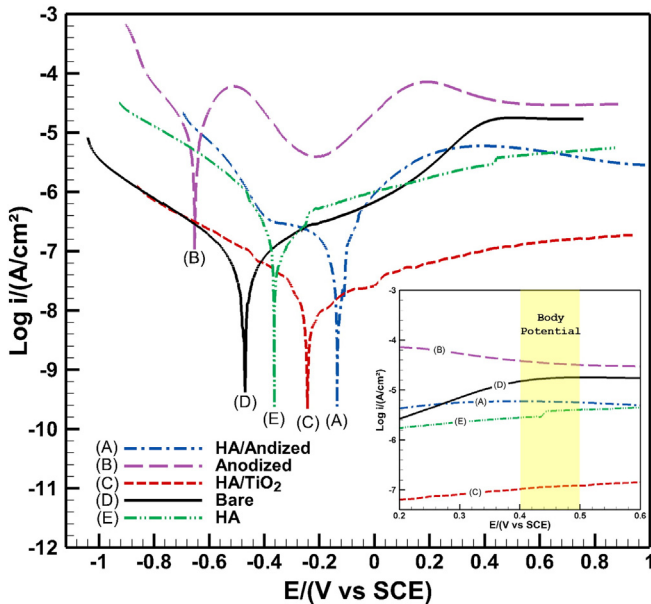


Fig. 7. (a) Polarization diagrams of different surface treated samples: (A) HA/anodized, (B) anodized, (C) HA/TiO₂ nanocomposite, (D) polished Ti6Al4V alloy (bare) and (E) hydroxyapatite coatings on Ti6Al4V alloy substrate. Polarization spectra of the samples in the range of body potential (400 to 500 mV) are also presented.

Table 2
Results of the polarization measurements in SBF solution at 37 °C.

Sample	Corrosion potential (mV vs SCE)	Passivation current density (μA/cm ²)
Bare	−475	18.96
Anodized	−651	32.28
HA	−364	3.93
HA/TiO ₂	−246	0.125
HA/Anodized	−134	5.53

resistance associated to the electrolyte solution relaxing at high frequencies. R_C and Q_C are the resistance and the constant phase element associated to the compact oxide layer ($R_{compact}$ and $Q_{compact}$ in Table 3), respectively. R_A and Q_A are the resistance and the constant-phase element associated with the anodized sample which consists of a TNT layer ($R_{Anodized}$ and $Q_{Anodized}$ in Table 3). R_{HA} and Q_{HA} present the resistance and the constant phase element associated to the deposited hydroxyapatite in each coated specimen. Also, R_{HT} and Q_{HT} are the resistance and the constant-phase element associated to the HA/TiO₂ nanocomposite coating ($R_{HA/Titania}$ and $Q_{HA/Titania}$ in Table 3), respectively.

The equivalent circuits allow a good agreement between the experimental data and the simulated impedance plots for comparative estimation of specific components of the studied surfaces. These surfaces belong to the untreated Ti6Al4V alloy, the anodized sample with nanotubular titanium oxide layer, the deposited hydroxyapatite, the HA/anodized and the HA/TiO₂ nanocomposite coating.

As is seen in the data of Table 3, the anodic TiO₂ nanotube layer consists of a thin inner compact and a barrier titanium oxide layer followed by an outer porous layer. This result confirms the data obtained by previous researchers [42]. With regard to the present porous structure (Fig. 3), the corrosion resistance of the anodized and the HA/anodized samples is lower than that of the other specimens (Figs. 7, 8 and 9).

From data of Table 3, hydroxyapatite increased the impedance resistance of the deposited layer. However, in the HA deposit, the polarization resistance is significantly lower than HA/TiO₂. This could be due to a porous heterogeneous microstructure like those shown in Fig. 4. This HA sample inhomogeneity could also be described by means of the parameter α of Eq. (1).

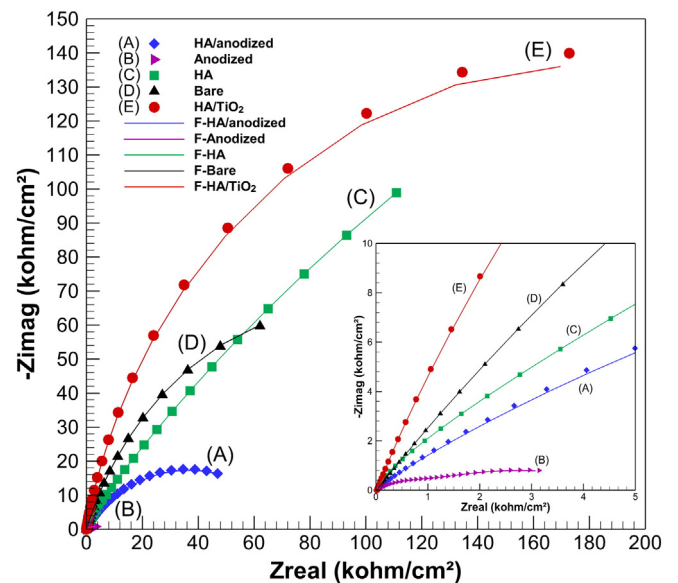


Fig. 8. The Nyquist diagrams of the samples in the SBF solution at 37 °C: (▲) bare Ti6Al4V, (◆) anodized alloy, (■) hydroxyapatite deposited, (◆) HA/anodized specimen and (●) HA/TiO₂ nanocomposite coated sample. Lines show the fitting curves of experimental data and are labeled by “F-sample name”.

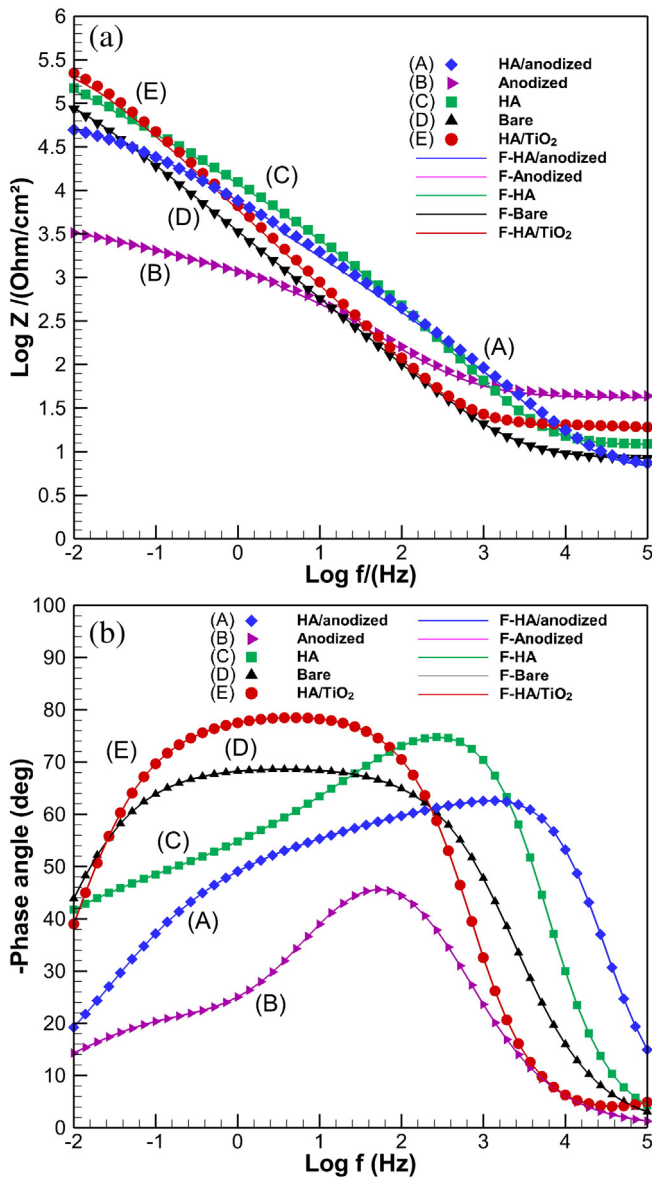


Fig. 9. (A) Bode plots and (B) phase angle diagrams as a function of frequency in logarithmic scale for (▲) untreated Ti6Al4V alloy, (▼) anodized, (■) hydroxyapatite deposited, (◆) HA/anodized and (●) HA/TiO₂ nanocomposite deposition. Lines show the fitting curves of experimental data and are labeled by "F-sample name".

The value of α corresponds to the linear slope modulus of Bode plot (Fig. 9a). It is well known that when m is near 1, the surface is uniform and smooth. On the other hand, lower values (in our case $m = 0.52$ in the HA coating specimen) shows deviation from ideal capacitive behavior (which has been attributed to the inhomogeneity of the surface) and deterioration of corrosion resistance [43,44]. Due to this result, the highest polarization resistance (extrapolation of Z modulus at low frequency) is obtained for interface formed on the Ti6Al4V alloy by electro-deposition of HA/TiO₂ (Fig. 9a). Furthermore, this result confirms the FE-SEM micrograph and shows that the lower density in the HA specimen is smaller than HA/TiO₂. Results show that with the addition of TiO₂ nanoparticles to the deposited layer, the surface density and the corrosion resistance increase.

3.5. X-ray diffraction

Fig. 11 compares the XRD patterns of Ti6Al4V alloy after anodization, HA deposition, HA/TiO₂ nanocomposite formation and HA/anodized

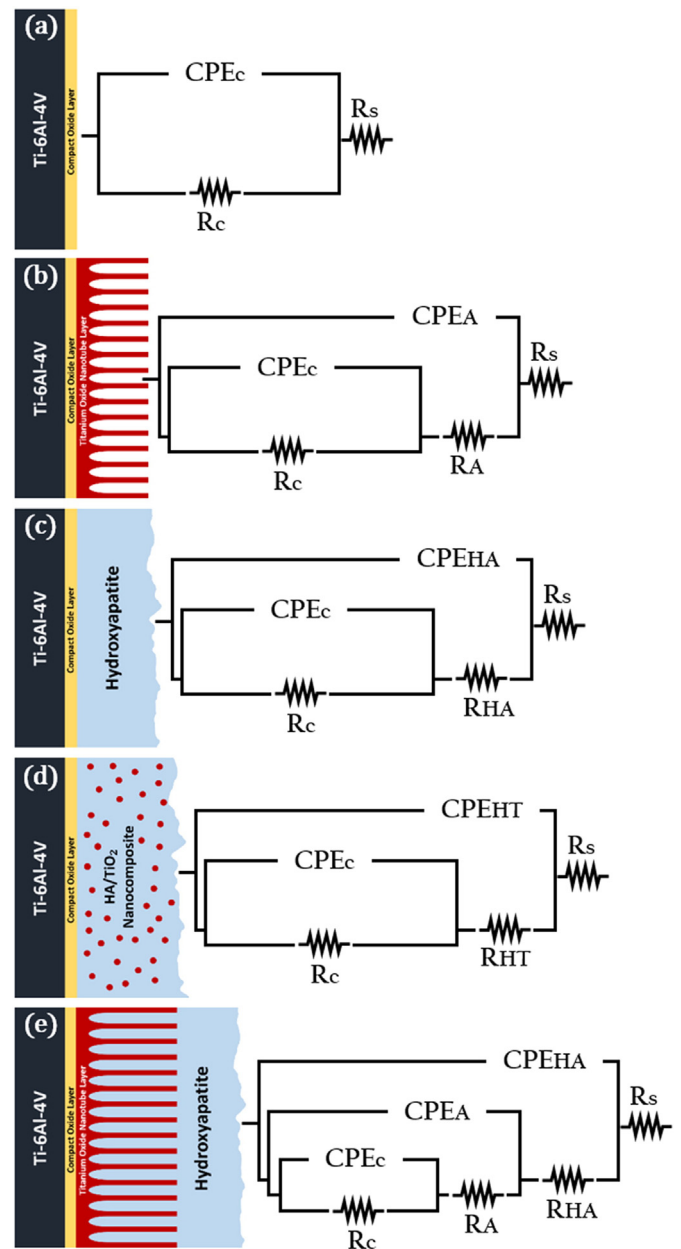


Fig. 10. Equivalent circuits representing the impedance results for the five surfaces to obtain the polarization resistance (R_p) values by fitting: (a) untreated Ti6Al4V alloy surface; (b) anodic porous TiO₂ layer surface; (c) deposited hydroxyapatite; (d) HA/TiO₂ nanocomposite coating and (e) HA/anodized layer specimen.

double layer production. As is seen, the oxide layer consists of an anatase TiO₂ phase which can be due to heat treatment at 480 °C at which an amorphous to anatase phase transformation occurs. Notice the sharp nanostructure peaks of a dense and compact TNT layer. The appearance of substrate peaks indicates the formation of a thin anodized layer.

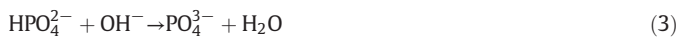
Fig. 11(2) shows a pure hydroxyapatite phase. It is interesting to note that the other calcium phosphate phases like octacalcium phosphate and tricalcium phosphate (TCP) which suffer lower stability, more dissolving rate and weaker biological response than hydroxyapatite [45] do not have considerable presence. According to Eliaz et al. [46], only if the pH value of the electrolyte is close to 11.6, will the pure hydroxyapatite be precipitated from the calcium phosphate electrolyte. They have demonstrated that at the presence of enough hydroxyl and phosphate ions in the electrolyte, a hydroxyapatite phase can form according to reaction (4) [46]. However, based on reactions 2 and 3, the

Table 3

Values of the elements of the electric equivalent circuits whose response fitted the data obtained for the untreated Ti6Al4V alloy, anodized, hydroxyapatite deposited, HA/anodized and HA/TiO₂ nanocomposite coatings.

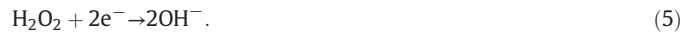
Elements of the electric equivalent circuits	Bare Ti6Al4V	Anodized	HA	HA/TiO ₂ nanocomposite	HA/Anodized
R _{Compact} /KΩ cm ²	187.7	14.7	637.8	872.5	66.4
Q _{Compact} /μF cm ⁻² s ^{α-1}	72.3	22.5	22.5	94.8	39.7
α _{Compact}	0.77	0.84	0.52	0.85	0.98
R _{Anodized} -R _{HA} -R _{HA/Titania} /KΩ cm ²	-	0.06	2.7	277.9	8
Q _{Anodized} -Q _{HA} -Q _{HA/Titania} /μF cm ⁻² s ^{α-1}	-	469.7	6.12	29.3	3.97
α _{Anodized} -α _{HA} -α _{HA/Titania}	-	0.24	0.9	0.88	0.56
R _{HA} /KΩ cm ²	-	-	-	-	0.044
Q _{HA} /μF cm ⁻² s ^{α-1}	-	-	-	-	2.3
α _{HA}	-	-	-	-	0.92
Chi-squared	1.65 × 10 ⁻⁶	4.85 × 10 ⁻⁴	3.24 × 10 ⁻⁶	6.25 × 10 ⁻⁴	2.23 × 10 ⁻⁵
(%)Mean error in Z	<1	<2.1	<1	<2.6	<1.8

formation of phosphate ions depends on the presence of hydroxyl ions [46–53].



Despite the above discussion, all samples were electrodeposited with CaP at pH = 5.5, consisting only of the HA phase. It is noteworthy that the presence of H₂O₂ in the electrolyte fulfills the need of reactions

(2) and (3) to hydroxyl (OH⁻) ions according to the following reaction [51,52]:

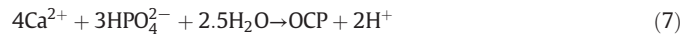


Formation of a pure hydroxyapatite phase is thus assisted with the presence of enough phosphate and hydroxyl ions, according to reaction (4).

Based on previous studies [50,51], in the electrodeposition process of CaP coatings under different conditions of an electrolyte solution, the following precipitation reactions (among others) may occur at the vicinity of the cathode:



or:



and Eq. (4) which leads to precipitation of the pure hydroxyapatite phase.

Among these four reactions, the probability for the occurrence of reaction (4) under the applied conditions in the present study is higher due to excessive OH⁻ ions as a result of reaction (5) and enough phosphate ions, which guarantee the occurrence of reaction (4). The most probable mechanism for the formation of hydroxyapatite coatings in the applied electrodeposition procedure of this study consists of a two-step process [54,55]: (I) when the voltage is applied, electrogenerated hydroxide ions are produced in the vicinity of the cathode during the precipitation process as well as phosphate ions; (II) the OH⁻, PO₄³⁻ and Ca²⁺ ions formed by the electrochemical reaction, react chemically at the appropriate pH and produce hydroxyapatite on the cathode surface. The OH⁻ ion concentration on the vicinity of the cathode affects the amount on the hydroxyapatite phase significantly. That is to say, the higher OH⁻ the concentration, the higher the amount of the HA phase [48]. The mechanism of pulsed electrodeposition for hydroxyapatite coatings on Ti6Al4V alloy has been presented in Fig. 12.

As shown in Fig. 12(a), when a pulsed current density was applied, H₂O₂ is first reduced into OH⁻ ions according to Eq. (5) [51,52] and leads to an increase in pH at the Ti6Al4V/electrolyte interface. Subsequently, Ca²⁺ and PO₄³⁻ ions in the vicinity of the cathode surface formed by reaction (3), react with OH⁻ ions to synthesize hydroxyapatite directly on the substrate surface (Fig. 12(b, c)) according to Eq. (4). With the HA forming, the concentration of PO₄³⁻ and Ca²⁺ ions near the electrode begins to decrease, but there is no change in the concentration of PO₄³⁻ and Ca²⁺ ions of bulk electrolyte near the vicinity of the electrode as shown in Fig. 12(b). The difference can lead to a concentration polarization which could influence the composition of deposition.

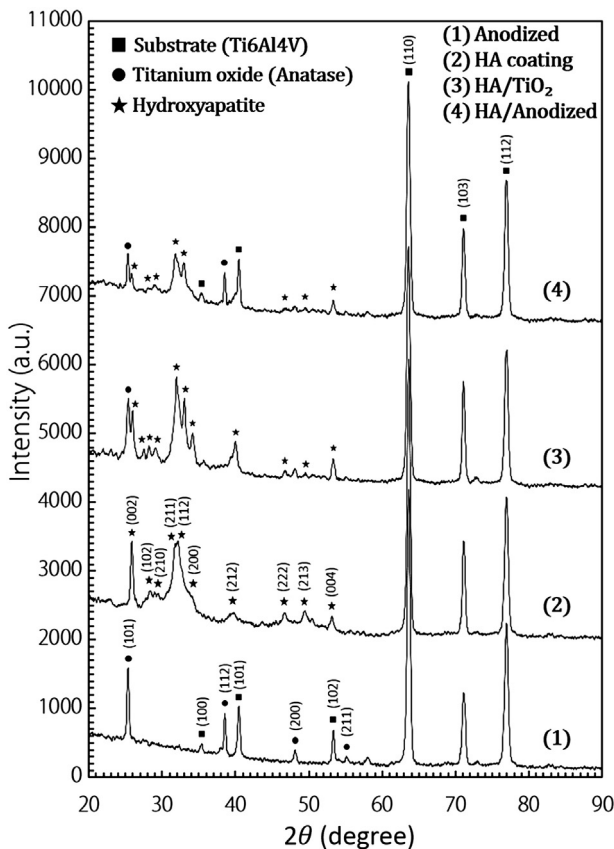


Fig. 11. X-ray diffraction patterns of the Ti6Al4V alloy: (1) anodized, (2) with HA deposit, (3) with HA/TiO₂ nanocomposite and (4) having HA/anodized double layers. The patterns are shifted 2000 units upwards with respect to the lower curve.

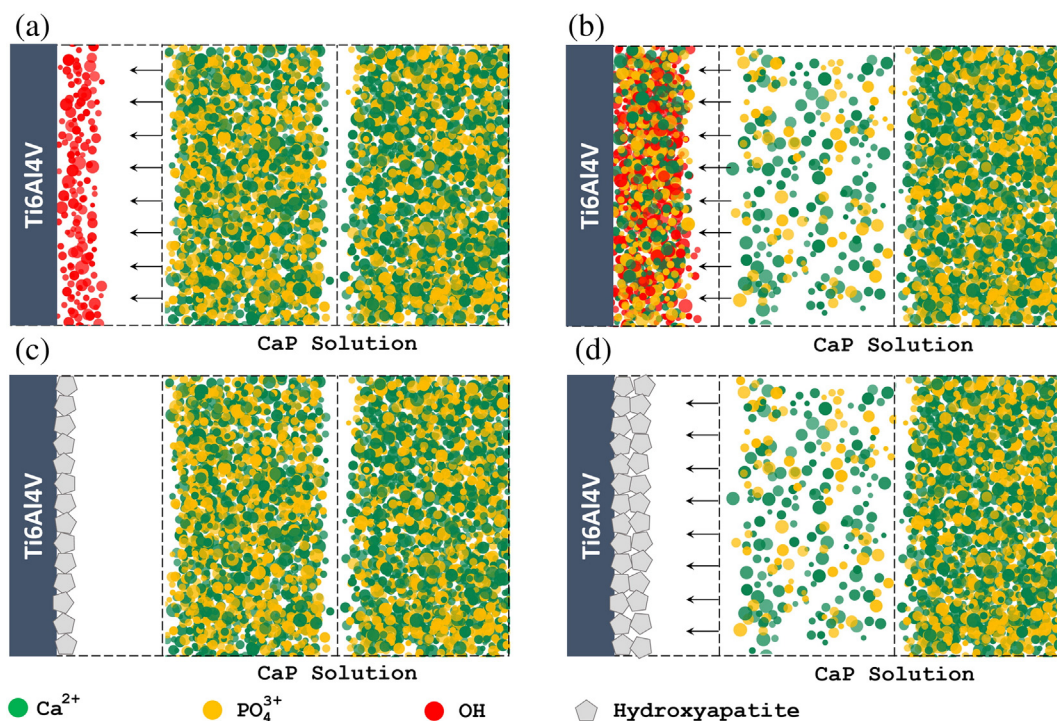


Fig. 12. Schematic for the mechanism of pulsed electrodeposition of hydroxyapatite coating. Panel (●) shows hydroxyl ions at the vicinity of cathode. Panels (●) and (●) represent the Ca^{2+} and PO_4^{3-} ions present in the electrolyte solution and the Ti6Al4V alloy substrate as cathode, during the application of pulsed on time (a and b), application of pulsed off time (c) and again the application of pulsed on time (d) respectively.

During the pulsed off time, i.e. in the relaxation time, when Ca^{2+} and PO_4^{3-} ions diffused from bulk electrolyte solution to the vicinity of the Ti6Al4V cathode (Fig. 12(c)), the polarization of concentration decreases. Again, when pulsed current density is applied, Ca^{2+} and PO_4^{3-} reacts with OH^- ions produced on the surface of the alloy to form hydroxyapatite as represented in Fig. 12(d). It means that when the pulsed current density is applied, polarization of concentration will be at its lowest level which results in the deposition of stoichiometric hydroxyapatite on the surface. Furthermore, this condition paves the way for the formation of a dense and strong coating having an appropriate adhesion to the substrate.

As is clear from Fig. 11, both diffraction patterns of the HA/TiO₂ and the HA/anodized layer consist of hydroxyapatite and anatase phases. However, intensities of the peaks relevant to different crystal planes are not the same. As is observed in Fig. 11, the (112) plane of the HA/anodized sample indicating the anatase TiO₂ layer is not seen in the HA/TiO₂ nanocomposite specimen. Meanwhile, the intensities of the HA peaks of the HA/anodized sample show a considerable decrease with respect to the HA/TiO₂ specimen. This can be due to the insulation effect of TiO₂ nanotubes. Based on previous works [56], the presence of a layer with weak conductivity can regulate the mobility of the depositing ions. This means that the presence of the intermediate TNT layer reduces the movement of HA producing ions (mentioned in reaction 4) toward the cathode surface. This decreases crystal-nucleation which lowers the crystallinity of the sample. On the other hand, the decrement of the ion mobility causes a lowering of the thickness and intensities of the peaks related to the HA.

4. Conclusions

The conditions applied to the electrodeposition of calcium phosphate components for the formation of highly pure hydroxyapatite phase were obtained. The presence of H₂O₂ in the electrolyte resulted in the release of the hydroxyl ion (OH^-) which contributed to the

phosphate ion production and eventual hydroxyapatite phase formation.

The high bonding strength of the HA/anodized layer was due to a highly rough surface topography which created strong mechanical interlocking, good wetting behavior of HA in contact with the anodized sample and high chemical affinity of HA against the Titania interlayer. Fair intermixing of the elements in the HA/Titania interface, however, formed weak bonds during heat treatment.

The measured bonding strength of the coatings that adhered to the substrate showed an increase of the adhesion strength by the addition of TiO₂ nanoparticles. A significant increase in HA/anodized adhesion strength was achieved due to the better wetting behavior of HA in contact with the anodized layer and interlocking of the roughened surface with HA colloidal particles which penetrated into the voids of the TiO₂ nanotubes.

Electrochemical studies showed the highest polarization resistance of HA/TiO₂ nanoparticles as compared to other samples. Pure hydroxyapatite electrochemically deposited on Ti6Al4V alloy improved the corrosion behavior of the substrate. The lowest passivation current density ($I_{\text{pass}} = 0.125 \mu\text{A}/\text{cm}^2$, less than 1% of that for the bare substrate) was obtained for the HA/TiO₂ nanocomposite coated specimen. Both anodized and HA/anodized-coated Ti6Al4V prototypes consisted of TNTs which showed weaker corrosion resistance than the HA and HA/TiO₂ samples. The poor corrosion behavior of TNTs was due to the void arrays that persuaded permeation of the corroding ions toward the interface. Although hydroxyapatite had fair corrosion resistance, its presence on the HA/anodized samples could not well enough improve poor corrosion behavior of the porous TNT layer.

Polarization curves evaluated in the range of body potential (400 mV–500 mV) and physiological environment showed lower corrosion current density for HA-based coated samples than the uncoated Ti6Al4V alloy. This meant that the deposition of hydroxyapatite and the production of the HA/TiO₂ nanocomposite and HA/anodized layer had a controlling effect on the surface behavior of Ti6Al4V alloy as an important candidate for biomedical applications.

Acknowledgments

The authors would like to gratefully appreciate the Iran Nanotechnology Initiative Council and the Research Council of the Sharif University of Technology for their general support.

References

- [1] X. Liu, P.K. Chu, C. Ding, Surface modification of titanium, titanium alloys, and related materials for biomedical applications, *Mater. Sci. Eng. R* 47 (2004) 49–121.
- [2] S. Ahmadi, S.K. Sadrnezhad, A novel method for production of foamy core@compact shell Ti6Al4V bone-like composite, *J. Alloys Compd.* 656 (2016) 416–422.
- [3] M. Geetha, A.K. Singh, R. Asokamani, A.K. Gogia, Ti based biomaterials, the ultimate choice for orthopaedic implants – a review, *Prog. Mater. Sci.* 54 (2009) 397–425.
- [4] S.N. Dezfouli, S.K. Sadrnezhad, M.A. Shokrgozar, S. Bonakdar, Fabrication of bio-compatible titanium scaffolds using space holder technique, *J. Mater. Sci. Mater. Med.* 23 (2012) 2483–2488.
- [5] M. Long, H.J. Rack, Titanium alloys in total joint replacement—a materials science perspective, *Biomaterials* 19 (1998) 1621–1639.
- [6] J. Ryhänen, M. Kallioinen, J. Tuukkanen, P. Lehenkari, J. Junila, E. Niemelä, P. Sandvik, W. Serlo, Bone modeling and cell–material interface responses induced by nickel–titanium shape memory alloy after periosteal implantation, *Biomaterials* 20 (1999) 1309–1317.
- [7] G. Rondelli, B. Vicentini, Localized corrosion behaviour in simulated human body fluids of commercial Ni–Ti orthodontic wires, *Biomaterials* 20 (1999) 785–792.
- [8] N.J. Hallab, K. Mikecz, C. Vermes, A. Skipor, J.J. Jacobs, Differential lymphocyte reactivity to serum-derived metal–protein complexes produced from cobalt-based and titanium-based implant alloy degradation, *J. Biomed. Mater. Res.* 56 (2001) 427–436.
- [9] D.J. Wever, A.G. Veldhuizen, J. de Vries, H.J. Busscher, D.R.A. Uges, J.R. van Horn, Electrochemical and surface characterization of a nickel–titanium alloy, *Biomaterials* 19 (1998) 761–769.
- [10] S. Minagar, C.C. Berndt, J. Wang, E. Ivanova, C. Wen, A review of the application of anodization for the fabrication of nanotubes on metal implant surfaces, *Acta Biomater.* 8 (2012) 2875–2888.
- [11] C.T. Kwok, P.K. Wong, F.T. Cheng, H.C. Man, Characterization and corrosion behavior of hydroxyapatite coatings on Ti6Al4V fabricated by electrophoretic deposition, *Appl. Surf. Sci.* 255 (2009) 6736–6744.
- [12] C.I. Jo, Y.H. Jeong, H.C. Choe, W.A. Brantley, Hydroxyapatite precipitation on nanotubular films formed on Ti6Al4V alloy for biomedical applications, *Thin Solid Films* 549 (2013) 135–140.
- [13] L. Benea, E. Mardare-Danaila, M. Mardare, J.P. Celis, Preparation of titanium oxide and hydroxyapatite on Ti–6Al–4V alloy surface and electrochemical behaviour in bio-simulated fluid solution, *Corros. Sci.* 80 (2014) 331–338.
- [14] C.K. Lee, Fabrication, characterization and wear corrosion testing of bioactive hydroxyapatite/nano-TiO₂ composite coatings on anodic Ti–6Al–4V substrate for biomedical applications, *Mater. Sci. Eng. B* 177 (2012) 810–818.
- [15] K. Sato, Mechanism of hydroxyapatite mineralization in biological systems, *J. Ceram. Soc. Jpn.* 115 (2007) 124–130.
- [16] M. Sadat-Shojai, M.T. Khorasani, E. Dinpanah-Khoshdargi, A. Jamshidi, Synthesis methods for nanosized hydroxyapatite with diverse structures, *Acta Biomater.* 9 (2013) 7591–7621.
- [17] A. Marten, P. Fratzl, O. Paris, P. Zaslansky, On the mineral in collagen of human crown dentine, *Biomaterials* 31 (2010) 5479–5490.
- [18] J. Takebe, S. Itoh, J. Okada, K. Ishibashi, Anodic oxidation and hydrothermal treatment of titanium results in a surface that causes increased attachment and altered cytoskeletal morphology of rat bone marrow stromal cells in vitro, *J. Biomed. Mater. Res.* 51 (2000) 398–407.
- [19] M. Aminzare, A. Eskandari, M.H. Baroonian, A.A. Berenov, Z. Razavi Hesabi, M. Taheri, S.K. Sadrnezhad, Hydroxyapatite nanocomposites: synthesis, sintering and mechanical properties, *Ceram. Int.* 39 (2013) 2197–2206.
- [20] K.S. Raja, M. Misra, K. Paramguru, Deposition of calcium phosphate coating on nanotubular anodized titanium, *Mater. Lett.* 59 (2005) 2137–2141.
- [21] L. Huang, K. Xu, J. Lu, A study of the process and kinetics of electrochemical deposition and the hydrothermal synthesis of hydroxyapatite coatings, *J. Mater. Sci.* 11 (2000) 667–673.
- [22] H. Arami, M. Mohajerani, M. Mazloumi, R. Khalifehzadeh, A. Lak, S.K. Sadrnezhad, Self-assembled dahlia-like cadmium hydrogen phosphate hydrate nanostructures as templates for cadmium hydroxyapatite hexagonal prisms, *J. Cryst. Growth* 309 (2007) 37–42.
- [23] D. Qiu, L. Yang, Y. Yin, A. Wang, Preparation and characterization of hydroxyapatite/titania composite coating on NiTi alloy by electrochemical deposition, *Surf. Coat. Technol.* 205 (2011) 3280–3284.
- [24] Z. Wu, L. He, Z. Chen, Composite biocoating of hydroxyapatite/Al₂O₃ on titanium formed by Al anodization and electrodeposition, *Mater. Lett.* 61 (2007) 2952–2955.
- [25] H. Farnoush, J. Aghazadeh-Mohandesib, H. Çimenoglu, Micro-scratch and corrosion behavior of functionally graded HA–TiO₂ nanostructured composite coatings fabricated by electrophoretic deposition, *J. Mech. Behav. Biomed. Mater.* 46 (2015) 31–40.
- [26] M. Goudarzi, F. Batmanghelich, A. Afshar, A. Dolati, G. Mortazavi, Development of electrophoretically deposited hydroxyapatite coatings on anodized nanotubular TiO₂ structures: corrosion and sintering temperature, *Appl. Surf. Sci.* 301 (2014) 250–257.
- [27] E. Mohseni, E. Zalnezhad, A.R. Bushroa, Comparative investigation on the adhesion of hydroxyapatite coating on Ti–6Al–4V implant: a review paper, *Int. J. Adhes. Adhes.* 48 (2014) 238–257.
- [28] P. Amaravathy, S. Sathyanarayanan, S. Sowndarya, N. Rajendran, Bioactive HA/TiO₂ coating on magnesium alloy for biomedical applications, *Ceram. Int.* 40 (2014) 6617–6630.
- [29] L. Benea, E. Mardare-Danaila, J.P. Celis, Increasing the tribological performances of Ti–6Al–4V alloy by forming a thin nanoporous TiO₂ layer and hydroxyapatite electrodeposition under lubricated conditions, *Tribol. Int.* 78 (2014) 168–175.
- [30] K.S. Brammer, C.J. Frandsen, S. Jin, TiO₂ nanotubes for bone regeneration, *Trends. Bioethanol.* 30 (2012) 315–322.
- [31] A.W. Tan, B. Pingguan-Murphy, R. Ahmad, S.A. Akbar, Review of Titania nanotubes: fabrication and cellular response, *Ceram. Int.* 38 (2012) 4421–4435.
- [32] J.M. Macak, K. Sirotna, P. Schmuki, Self-organized porous titanium oxide prepared in Na₂SO₄/NaF electrolytes, *Electrochim. Acta* 50 (2005) 3679–3684.
- [33] S.P. Albu, A. Ghicov, S. Aldabergenova, P. Drechsel, D. LeClere, G.E. Thompson, J.M. Macak, P. Schmuki, Formation of double-walled TiO₂ nanotubes and robust anatase membranes, *Adv. Mater.* 20 (2008) 4135–4139.
- [34] A. Tighineanu, T. Ruff, S.P. Albu, R. Hahn, P. Schmuki, Conductivity of TiO₂ nanotubes: influence of annealing time and temperature, *Chem. Phys. Lett.* 494 (2010) 260–263.
- [35] A. Ghicov, H. Tsuchiya, J.M. Macak, P. Schmuki, Annealing effects on the photoresponse of TiO₂ nanotubes, *Phys. Status Solidi A* 203 (2006) R28–R30.
- [36] P.C. Rath, L. Besra, B.P. Singh, S. Bhattacharjee, Titania/hydroxyapatite bi-layer coating on Ti metal by electrophoretic deposition: characterization and corrosion studies, *Ceram. Int.* 38 (2012) 3209–3216.
- [37] A.J. Bard, L.R. Faulkner, *Electrochemical Methods, Fundamentals and Applications*, John Wiley & Sons, New York, 2001.
- [38] E.E. Stansbury, R.A. Buchanan, *Fundamentals of Electrochemical Corrosion*, ASM International, Materials Park, Ohio, 2000.
- [39] H. Anawati, H. Tanigawa, T. Asoh, M. Ohno, S. Ono Kubota, Electrochemical corrosion and bioactivity of titanium–hydroxyapatite composites prepared by spark plasma sintering, *Corros. Sci.* 70 (2013) 212–220.
- [40] D. Velten, V. Biehl, F. Aubertin, B. Valeske, W. Possart, J. Brems, Preparation of TiO₂ layers on cp-Ti and Ti6Al4V by thermal and anodic oxidation and by sol–gel coating techniques and their characterization, *J. Biomed. Mater. Res.* 59 (2002) 18–28.
- [41] L.T. Duarte, S.R. Biaggio, R.C. Rocha-Filho, N. Bocchi, Preparation and characterization of biomimetically and electrochemically deposited hydroxyapatite coatings on micro-arc oxidized Ti–13Nb–13Zr, *J. Mater. Sci. Mater. Med.* 22 (2011) 1663–1670.
- [42] R. Bholra, B. Mishra, in: T. Chandra, M. Ionescu, D. Mantovani (Eds.), Characterization of a Biomedical Titanium Alloy Using Various Surface Modifications to Enhance its Corrosion Resistance and Biocompatibility, *Mater. Sci. Forum, THERMEC 2011*, 706–709 2011, pp. 105–112.
- [43] P.L. Cabot, J.A. Garrido, E. Perez, A.H. Moreira, P.T.A. Sumodjo, W. Proud, EIS study of heat-treated Al–Zn–Mg alloys in the passive and transpassive potential regions, *Electrochim. Acta* 40 (1995) 447–454.
- [44] I. Mohammadi, A. Afshar, Modification of nanostructured anodized aluminum coatings by pulse current mode, *Surf. Coat. Technol.* 278 (2015) 48–55.
- [45] D.N. Misra, Adsorption on and Surface Chemistry of Hydroxyapatite, *American Chemical Society*, 1984.
- [46] N. Eliaz, T.M. Sridhar, Electrocrystallization of hydroxyapatite and its dependence on solution conditions, *Cryst. Growth Des.* 8 (2008) 3965–3977.
- [47] E.A. Abdel-Aal, D. Dietrich b, S. Steinhäuser b, B. Wielage, Electrocrystallization of nanocrystalline calcium phosphate coatings on titanium substrate at different current densities, *Surf. Coat. Technol.* 202 (2008) 5895–5900.
- [48] Q. Yuan, T.D. Golden, Electrochemical study of hydroxyapatite coatings on stainless steel substrates, *Thin Solid Films* 518 (2009) 55–60.
- [49] S.K. Yen, C.M. Lin, Cathodic reactions of electrolytic hydroxyapatite coating on pure titanium, *Mater. Chem. Phys.* 77 (2002) 70–76.
- [50] N. Eliaz, Electrocrystallization of calcium phosphates, *Isr. J. Chem.* 48 (2008) 159–168.
- [51] R. Dreveta, H. Benhayoune, L. Worthama, S. Potirona, J. Dougladeb, D. Laurent-Maquina, Effects of pulsed current and H₂O₂ amount on the composition of electro-deposited calcium phosphate coatings, *Mater. Charact.* 61 (2010) 786–795.
- [52] D. Gopi a,b, J. Indira a, L. Kavitha, A comparative study on the direct and pulsed current electrodeposition of hydroxyapatite coatings on surgical grade stainless steel, *Surf. Coat. Technol.* 206 (2012) 2859–2869.
- [53] P. Marco Antonio Lopez-Heredia, W.P. Layrolle, An electrodeposition method of calcium phosphate coatings on titanium alloy, *J. Mater. Sci. Mater. Med.* 18 (2007) 381–390.
- [54] G.H.A. Therese, P.V. Kamath, G.N. Subbanna, Novel electrochemical route to calcium phosphate coatings, *J. Mater. Chem.* 8 (1998) 405–408.
- [55] P. Zhu, Y. Masuda, K. Koumoto, The effect of surface charge on hydroxyapatite nucleation, *Biomaterials* 25 (2004) 3915–3921.
- [56] R. Femmer, A. Mani, M. Wessling, Ion transport through electrolyte/polyelectrolyte multi-layers, *Sci. Rep.* 4 (2015), 11583 <http://dx.doi.org/10.1038/srep11583>.